



# CHORUS

This is the accepted manuscript made available via CHORUS. The article has been published as:

## Trimerization and orbital ordering in $\text{Ba}_{1-x}\text{Sr}_x\text{V}_{13}\text{O}_{18}$

T. Kajita, Y. Obata, Y. Kakesu, Y. Imai, Y. Shmizu, M. Itoh, H. Kuwahara, and T. Katsufuji

Phys. Rev. B **96**, 245126 — Published 21 December 2017

DOI: [10.1103/PhysRevB.96.245126](https://doi.org/10.1103/PhysRevB.96.245126)

# Trimerization and orbital ordering in $\text{Ba}_{1-x}\text{Sr}_x\text{V}_{13}\text{O}_{18}$

T. Kajita,<sup>1</sup> Y. Obata,<sup>1</sup> Y. Kakesu,<sup>1</sup> Y. Imai,<sup>2</sup> Y.

Shmizu,<sup>2</sup> M. Itoh,<sup>2</sup> H. Kuwahara,<sup>3</sup> and T. Katsufuji<sup>1,4</sup>

<sup>1</sup>*Department of Physics, Waseda University, Tokyo 169-8555, Japan*

<sup>2</sup>*Department of Physics, Nagoya University, Chikusa, Nagoya 464-8602, Japan*

<sup>3</sup>*Department of Physics, Sophia University, Tokyo 102-8554, Japan*

<sup>4</sup>*Kagami Memorial Laboratory for Material Science and Technology,*

*Waseda University, Tokyo 169-0051, Japan*

(Dated: October 3, 2017)

## Abstract

We studied the physical properties of  $\text{Ba}_{1-x}\text{Sr}_x\text{V}_{13}\text{O}_{18}$  single crystals, which exhibit three different phases caused by the orbital and charge degrees of freedom in V  $t_{2g}$  states. We found from the magnetic susceptibility and the NMR measurement that the low-temperature phase of this series of compounds is characterized by the spin-singlet state. We also found from the electrical resistivity and optical conductivity spectra that these compounds become heavily anisotropic in the low-temperature phase with V trimerization, indicating that the orbital ordering of V  $t_{2g}$  states causes the anisotropy of the electronic structure of this series of compounds.

PACS numbers: 75.25.Dk,78.30.-j,72.80.Ga,76.60.-k

## I. INTRODUCTION

Vanadium oxides with one or two  $d$  electrons in  $t_{2g}$  states exhibit various interesting ordered states arising from the orbital degree of freedom of the  $d$  electrons. For example,  $\text{LiVO}_2$  with  $\text{V}^{3+}$  ( $3d^2$ ) ions on a triangular lattice exhibits the trimerization of V ions at  $\sim 460$  K, causing a sharp decrease in magnetic susceptibility.<sup>1-3</sup> It was proposed by Pen *et al.* that such trimerization is caused by the orbital ordering of  $t_{2g}$  states on V ions and the formation of a spin-singlet bond at each edge of the V trimer,<sup>4</sup> as shown in Fig. 1(a).

Recently, it has been found that  $\text{BaV}_{10}\text{O}_{15}$  (in which the average valence of V is +2.8)<sup>5-8</sup>,  $\text{Ba}_2\text{V}_{13}\text{O}_{22}$  (+3.08)<sup>9</sup>, and  $\text{Ba}_{1-x}\text{Sr}_x\text{V}_{13}\text{O}_{18}$  (+2.63)<sup>10-12</sup> with V ions on a quasi-triangular lattice exhibit ordered states similar to that of  $\text{LiVO}_2$ . For example, the trimerization of V ions occurs in  $\text{BaV}_{10}\text{O}_{15}$  at 123 K, causing the opening of a charge gap of  $\sim 0.3$  eV and a sharp increase in resistivity by three orders of magnitude.<sup>6</sup> A similar phase transition with V trimerization accompanied by a sharp decrease in magnetic susceptibility is observed in  $\text{Ba}_2\text{V}_{13}\text{O}_{22}$  but at a higher temperature of  $\sim 290$  K.<sup>9</sup>

It should be pointed out that these vanadates with mixed-valent V ions also has the charge degree of freedom of the  $d$  electrons, unlike  $\text{LiVO}_2$  with only  $\text{V}^{3+}$  ions, and this results in a wider variety of phase transitions. In this respect,  $\text{Ba}_{1-x}\text{Sr}_x\text{V}_{13}\text{O}_{18}$  with a hexagonal structure, in which V ions form a quasi-fcc lattice, are an intriguing series of compounds since they exhibit three different phases with temperatures,<sup>10,11</sup> as shown in Fig. 2. For  $\text{BaV}_{13}\text{O}_{18}$ , the high-temperature (HT) phase is characterized by the magnetic susceptibility  $\chi$  that decreases with decreasing  $T$ , and also by a structural distortion, in which six V tetramers in a rhombus shape surround one center V ion, as illustrated in Fig. 1(c). In this V tetramer, there are five V–V bonds, each of which presumably consists of two V  $t_{2g}$  states in a spin singlet state [Fig. 1(b)]; namely, the orbital ordering of the V  $t_{2g}$  states occurs in this HT phase. With decreasing temperature, the transition from the HT phase to the intermediate temperature (IT) phase occurs at  $T_{co} \sim 200$  K, and the IT phase is characterized by the Curie–Weiss behavior of magnetic susceptibility and the doubling of a unit cell, although the basic structure of the V tetramers is unchanged. These results suggest the charge ordering of the localized  $d$  electrons on the center V ion in the IT phase, though there are still itinerant electrons in this phase, as described below. With further decrease in temperature, another transition from the IT phase to the low-temperature (LT)

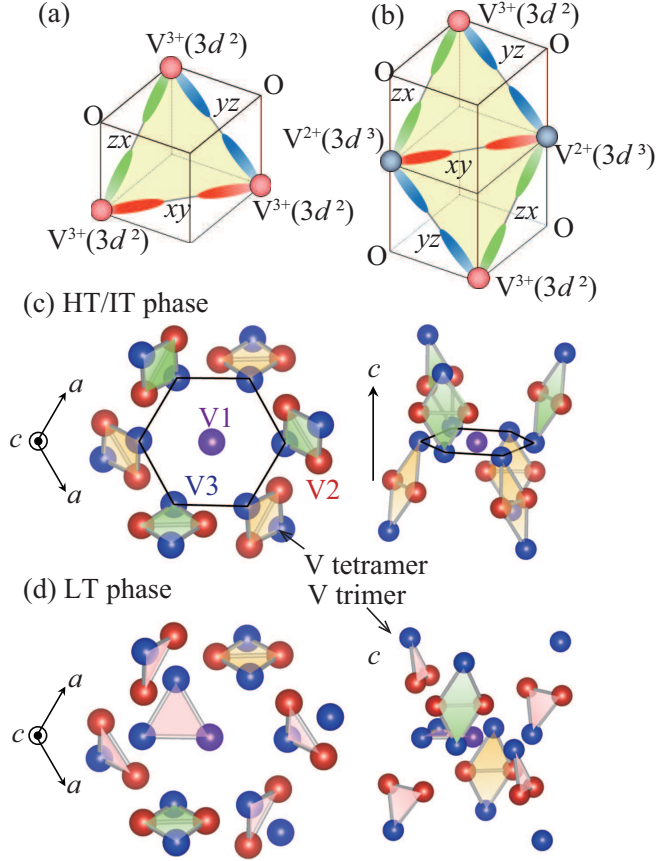


FIG. 1: (Color online) (a)(b) Schematic illustrations of orbital ordering in (a) V trimer and (b) V tetramer. (c) Arrangement of V ions in HT and IT phases viewed along  $c$ -axis (left) and  $ab$  plane (right). (d) Arrangement of V ions in LT phase viewed along  $c$ -axis (left) and  $ab$  plane (right). (c) and (d) are drawn using VESTA.<sup>13</sup>

phase occurs at  $T_{\text{tr}} \sim 70$  K. In the HT and the IT phases, there are three V tetramers and one center V ion in a unit cell (13 V ions), but they change into three V trimers and one V tetramer in the LT phase [Fig. 1(d)]. It is speculated that each bond of a V trimer consists of two V  $t_{2g}$  states in a spin singlet state [Fig. 1(a)].<sup>4</sup> With increasing Sr concentration,  $x$ , in  $\text{Ba}_{1-x}\text{Sr}_x\text{V}_{13}\text{O}_{18}$ ,  $T_{\text{co}}$  decreases, whereas  $T_{\text{tr}}$  increases, and the IT phase for  $T_{\text{tr}} < T < T_{\text{co}}$  eventually disappears and the transition from the HT phase to the LT phase occurs in the region of  $x > 0.3$ . This behavior indicates a competition between the IT and LT phases in this series of compounds.

Previous studies on  $\text{Ba}_{1-x}\text{Sr}_x\text{V}_{13}\text{O}_{18}$  were performed mainly using polycrystalline samples,<sup>10,11</sup> and studies using single crystals were carried out only on  $\text{BaV}_{13}\text{O}_{18}$ .<sup>12</sup> In this

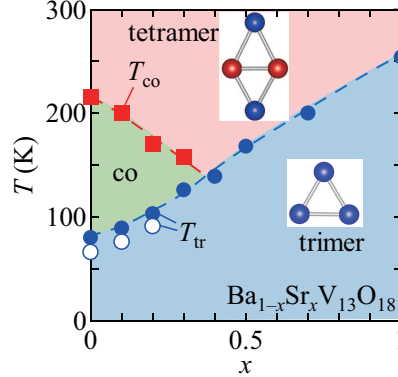


FIG. 2: (Color online) Phase diagram of the  $\text{Ba}_{1-x}\text{Sr}_x\text{V}_{13}\text{O}_{18}$  single crystals. The closed squares correspond to the transition temperatures between the HT phase and the IT phase. The circles correspond to the transition temperatures between the IT phase and LT phase ( $x \leq 0.3$ ) or between the HT phase and LT phase ( $x > 0.3$ ). The closed and opened circles correspond to that in the warming and cooling run, respectively.

study, we investigated the physical properties of  $\text{Ba}_{1-x}\text{Sr}_x\text{V}_{13}\text{O}_{18}$  single crystals. In particular, we focused on how the anisotropy of the electronic structural changes with different phases and the Sr concentration  $x$ .

## II. EXPERIMENT

We grew  $\text{Ba}_{1-x}\text{Sr}_x\text{V}_{13}\text{O}_{18}$  single crystals by the floating zone technique. Details were described elsewhere.<sup>12</sup> Electrical resistivity was measured using a conventional four-probe method. Magnetic susceptibility was measured using a SQUID magnetometer. Hall coefficient was measured at applied magnetic fields of up to 7 T by using a superconducting magnet. Optical reflectivity on a cleaved surface along the  $(32\bar{2})$  plane was measured using a FTIR spectrometer between 0.07 and 0.8 eV, and a grating spectrometer between 0.7 and 5 eV for the temperature range between 300 and 30 K with a He-gas-flow cryostat. The optical conductivity spectra  $\sigma(\omega)$  were obtained by the Kramers–Kronig transformation of reflectivity spectra with a constant extrapolation of the reflectivity below 0.07 eV and a constant extrapolation between 5 eV and 20 eV and an  $\omega^{-4}$  extrapolation above. The way of obtaining  $\sigma(\omega)$  along the  $a$  and the  $c$  axis from the reflectivity spectra on the surface along such an oblique  $(32\bar{2})$  plane was described in Ref. [12]. <sup>51</sup>V NMR spectra and nuclear

spin-lattice relaxation rate were measured for  $x = 0$  and  $x = 0.1$  samples at a constant magnetic field of 6.10 T.

### III. RESISTIVITY, MAGNETIC SUSCEPTIBILITY, AND HALL MEASUREMENT

Figures 3 (a)–(d) show the resistivity  $\rho$  of the  $\text{Ba}_{1-x}\text{Sr}_x\text{V}_{13}\text{O}_{18}$  single crystals with  $x = 0, 0.1, 0.2$ , and 1 along the  $a$ -axis ( $\rho_a$ ) and  $c$ -axis ( $\rho_c$ ). At 300 K, the magnitudes of  $\rho_a$  and  $\rho_c$  are comparable and both increase with decreasing temperature ( $T$ ). When  $x \leq 0.2$ ,  $\rho_a(T)$  and  $\rho_c(T)$  exhibit small anomalies at  $T_{\text{co}}$  (closed triangles).  $\rho_a(T)$  and  $\rho_c(T)$  from 300 K to  $T_{\text{co}}$  can be fitted on the basis of the thermal activation-type  $T$  dependence,  $\rho = \rho_0 \exp(E_g/k_B T)$ , and the activation energy  $E_g$  is plotted as a function of  $x$  in Fig. 3(f). As can be seen,  $E_g/k_B$  is comparable to  $T_{\text{co}}$ . Below  $T_{\text{co}}$  in the IT phase, the increases in  $\rho_a(T)$  and  $\rho_c(T)$  with decreasing  $T$  become less significant, and they rather decrease with decreasing  $T$  for  $x = 0$  and 0.1, typical of a metallic state.

With further decrease in  $T$  when  $x \leq 0.2$ ,  $\rho_a(T)$  sharply decreases, whereas  $\rho_c(T)$  sharply increases with a  $T$  hysteresis at  $T_{\text{tr}}$  (open triangles), and below  $T_{\text{tr}}$  in the LT phase, both  $\rho_a(T)$  and  $\rho_c(T)$  increase with decreasing  $T$ , but the increase is more significant for  $\rho_c(T)$ . For  $\text{SrV}_{13}\text{O}_{18}$ , where  $T_{\text{co}}$  is no more existing,  $\rho_a(T)$  sharply decreases, whereas  $\rho_c(T)$  sharply increases at  $T_{\text{tr}} \sim 250$  K [the inset of Fig. 3 (d)], and  $\rho_a$  is almost  $T$ -independent, whereas  $\rho_c$  increases with decreasing  $T$  below  $T_{\text{tr}}$  in the LT phase. Such an anisotropic behavior of  $\rho(T)$  in the LT phase for  $\text{Ba}_{1-x}\text{Sr}_x\text{V}_{13}\text{O}_{18}$  will be discussed later together with the anisotropy of optical conductivity. It should be pointed out that the decrease in  $\rho(T)$  at  $T_{\text{tr}}$  with decreasing  $T$  for the polycrystalline samples<sup>11</sup> is dominated by the behavior of  $\rho_a(T)$  for the single crystals.

Figure 3 (e) shows the magnetic susceptibility  $\chi(T)$  of the  $\text{Ba}_{1-x}\text{Sr}_x\text{V}_{13}\text{O}_{18}$  single crystals. As shown for  $\text{BaV}_{13}\text{O}_{18}$ , the anisotropy in  $\chi(T)$  between  $H \parallel a$  ( $\chi_a$ ) and  $H \parallel c$  ( $\chi_c$ ) is barely observed in the entire temperature range, unlike that in  $\rho(T)$ . When  $x \leq 0.3$ ,  $\chi(T)$  decreases with decreasing  $T$  from 300 K to  $T_{\text{co}}$  in the HT phase. As discussed in the introduction, this can be attributed to the spin-gap behavior dominated by the thermal excitation from the spin-singlet state to the spin-triplet state in the V–V bonds of the V tetramers [Fig. 1(c)].

At  $T_{\text{co}}$  (closed triangles),  $\chi(T)$  exhibits a small drop and below  $T_{\text{co}}$  in the IT phase, it

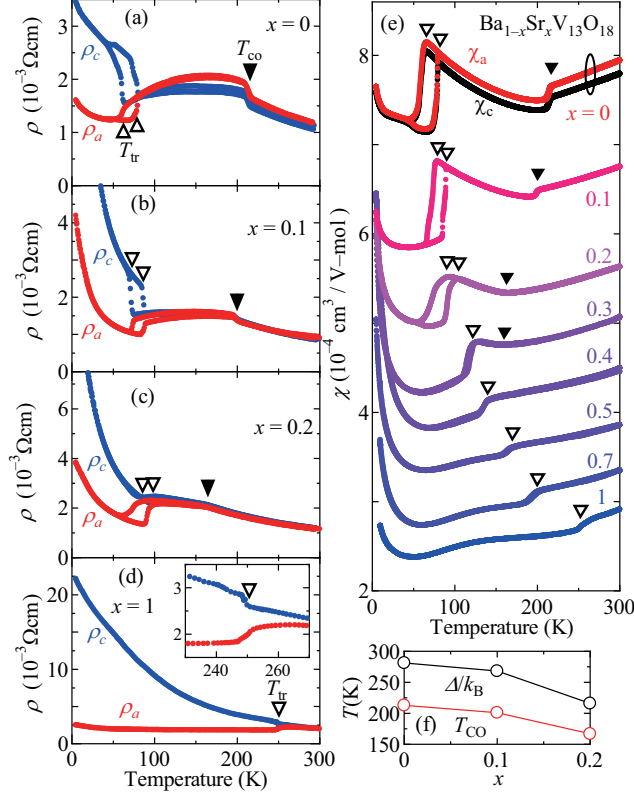


FIG. 3: (Color online) (a)(b)(c)(d) Temperature dependence of the resistivity for  $\text{Ba}_{1-x}\text{Sr}_x\text{V}_{13}\text{O}_{18}$  with (a)  $x = 0$ , (b)  $x = 0.1$ , (c)  $x = 0.2$ , and (d)  $x = 1$ . (e) Temperature dependence of the magnetic susceptibility for  $\text{Ba}_{1-x}\text{Sr}_x\text{V}_{13}\text{O}_{18}$ . The data are offset for clarity. (f) Sr concentration dependences of  $E_g/k_B$  and  $T_{CO}$

obeys the Curie–Weiss behavior, which can be attributed to the local magnetic moment at the center V ion. To estimate the local magnetic moment in the IT phase of  $\text{Ba}_{1-x}\text{Sr}_x\text{V}_{13}\text{O}_{18}$  ( $x = 0, 0.1,$  and  $0.2$ ),  $\chi(T)$  was fitted using  $\chi(T) = \chi_v + C/(T + \theta)$ , where  $\chi_v$  is a  $T$ -independent paramagnetic term (Van Vleck term) and the second term is a Curie–Weiss term with the Curie constant  $C$  and the Weiss temperature  $\theta$ . The  $\chi_v$  value of  $\sim 1 \times 10^{-4} \text{cm}^3/\text{V-mol}$  is comparable to those of  $\text{LiVO}_2$ <sup>14</sup> and  $\text{V}_2\text{O}_3$ <sup>15</sup>. The Curie constant  $C$  obtained by fitting is in the range of  $1.1 - 1.5 \times 10^{-2} \text{cm}^3\text{K}/\text{V-mol}$  for  $x = 0 - 0.2$ .

At  $T_{tr}$  (open triangle),  $\chi(T)$  sharply decreases and shows an almost  $T$ -independent behavior below  $T_{tr}$ , although a small amount of a Curie term appears below 30 K. This sharp decrease in  $\chi(T)$  at  $T_{tr}$ , which is much more prominent than that for the polycrystalline samples<sup>11</sup> and is accompanied by a  $T$  hysteresis, is caused by V trimerization and the suppression of the magnetic moment on the center V ion.

With increasing  $x$  for  $\text{Ba}_{1-x}\text{Sr}_x\text{V}_{13}\text{O}_{18}$ ,  $T_{\text{co}}$  decreases, whereas  $T_{\text{tr}}$  increases, and when  $x \geq 0.4$ ,  $T_{\text{co}}$  and  $T_{\text{tr}}$  merge and the Curie–Weiss behavior disappears. We draw the phase diagram of the  $\text{Ba}_{1-x}\text{Sr}_x\text{V}_{13}\text{O}_{18}$  single crystals in Fig. 2, where  $T_{\text{co}}$  and  $T_{\text{tr}}$  are obtained from the magnetic susceptibility data. The result is similar to that of the polycrystalline samples previously reported,<sup>11</sup> except for the behavior at  $x = 0$ . In the case of the polycrystalline samples, though  $T_{\text{tr}}$  exists in  $\text{Ba}_{1-x}\text{Sr}_x\text{V}_{13}\text{O}_{18}$  with finite values of  $x$ , no anomaly corresponding to  $T_{\text{tr}}$  was observed for  $\text{BaV}_{13}\text{O}_{18}$ .<sup>11</sup> According to the studies on the single crystals, the stoichiometric  $\text{BaV}_{13}\text{O}_{18}$  crystal exhibits  $T_{\text{tr}}$  whereas the offstoichiometric one does not.<sup>12</sup> It is likely that this results in the different behaviors at  $x = 0$  between the polycrystalline samples and the single crystals.

The Hall coefficient  $R_H$  with  $j \parallel c$  and  $H \parallel a$  for  $\text{BaV}_{13}\text{O}_{18}$  as a function of  $T$  is shown in Fig. 4.  $R_H$  above  $T_{\text{tr}}$  (in the IT phase) is negative and the absolute value immediately above  $T_{\text{tr}} = 60$  K is  $\sim 2 \times 10^{-3}$  cm<sup>3</sup>/C, which corresponds to 0.07 electron per V ion. In  $\text{Ba}_{1-x}\text{Sr}_x\text{V}_{13}\text{O}_{18}$ , there are 31  $d$  electrons per 13 V ions, and in the IT phase, 30 electrons can be accommodated in the three V tetramers (each of which has five bonds and can accommodate ten electrons); thus, one  $d$  electron should exist on the center V ion. However, part of this electron should be localized and contributes to the Curie–Weiss behavior of magnetic susceptibility. Thus, one possible scenario for the IT phase is that some  $d$  electrons on the center V ion are localized and contribute to the Curie–Weiss behavior, whereas the others are itinerant and contribute to the Hall coefficient. The doubling of the unit cell observed in the electron diffraction<sup>10</sup> seems to support this idea. Furthermore, the Curie constant experimentally obtained ( $1.1 - 1.5 \times 10^{-2}$  cm<sup>3</sup>K/V-mol) is comparable to that obtained when a  $S=1/2$  spin exists per doubled unit cell (26V),  $C = 1.4 \times 10^{-2}$  cm<sup>3</sup>K/V-mol. The number of the itinerant electrons in the IT phase estimated from the Hall coefficient above ( $\sim 0.07$ ) seems compatible with the number of the carriers in this model,  $1/26 \sim 0.038$ .

With decreasing  $T$ ,  $R_H$  sharply drops to  $-8 \times 10^{-3}$  cm<sup>3</sup>/C at 56 K (immediately below  $T_{\text{tr}} = 60$  K), and with further decrease in  $T$ ,  $R_H$  starts to increase below 20 K, and the sign of  $R_H$  changes from negative to positive at 12 K and reaches  $1.4 \times 10^{-2}$  cm<sup>3</sup>/C at the lowest temperature of 2 K. The change in sign indicates that, in the LT phase, two kinds of carriers, namely, holes and electrons, exist. In the case of charge-density-wave (CDW) compounds<sup>16,17</sup>, the sign of Hall coefficient changes from positive to negative at the CDW phase transition accompanied by nesting of Fermi surface. In Ru oxides, such as

$\text{Sr}_2\text{RuO}_4$ <sup>18-20</sup>,  $\text{SrRuO}_4$ <sup>21</sup>, and  $\text{Ba}_4\text{Ru}_3\text{O}_{10}$ <sup>22</sup>, the complicated band structures cause the sign inversion of Hall coefficient with temperature.

The number of carriers estimated from  $R_H$  at 56 K is  $\sim 0.02$  electrons per V. In the LT phase, there are 31  $d$  electrons per 13 V ions and 28 electrons can be accommodated in one V tetramer (which can accommodate ten electrons) and three V trimers (each of which can accommodate six electrons). Thus, three electrons do not form a bonding state but should be itinerant. However, the number of electrons per V experimentally estimated ( $\sim 0.02$ ) is much smaller than that expected from such a simple model discussed above,  $3/13 \sim 0.23$ . Furthermore, this model cannot explain the existence of both holes and electrons. These two results suggest that complex Fermi surfaces exist in the LT phase of this series of compounds.

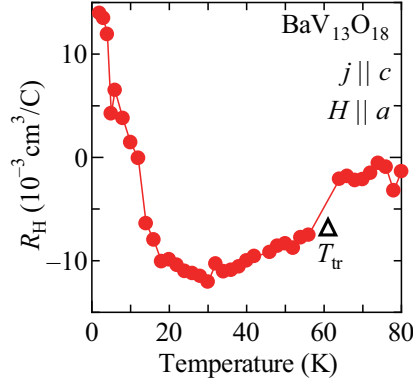


FIG. 4: (Color online) Temperature dependence of Hall coefficient for  $\text{BaV}_{13}\text{O}_{18}$ .

#### IV. NMR MEASUREMENT

To obtain microscopic insights into the ground state, the  $^{51}\text{V}$  NMR spectrum was measured on the single crystal of the  $x = 0$  sample for the magnetic field of 6.10 T along the  $c$ -axis, as shown in Fig. 5(a). We observed one set of the nonmagnetic NMR spectra with small quadrupole splitting for the nuclear spin  $I = 7/2$  at 300 K. The observed nonmagnetic V site can be V2 among the tetramers in the HT phase, since the V2–V2 bond is much shorter than the V2–V3 bond. The spectrum from V1 and V3 are wiped out due to the fast nuclear spin relaxation rates in the HT phase. The shape of the spectrum clearly changes across  $T_{\text{co}}$  and  $T_{\text{tr}}$ . At 190 K below  $T_{\text{co}}$ , the spectrum becomes complex with the decrease

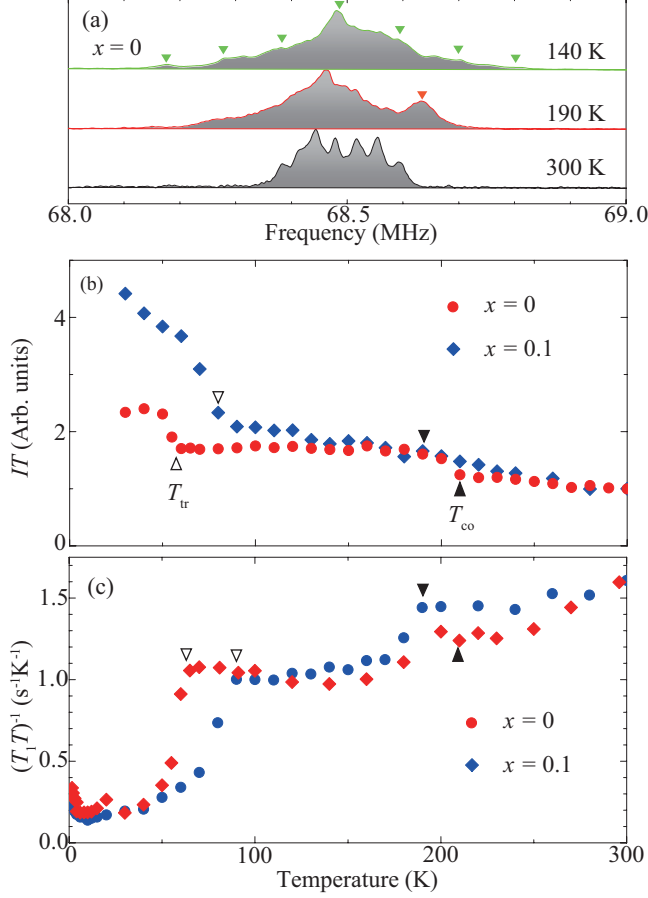


FIG. 5: (Color online) (a)  $^{51}\text{V}$  NMR spectra of  $\text{BaV}_{13}\text{O}_{18}$  for  $H \parallel c$ . The intensity of the spectra is normalized using the peak value. The Knight shift origin ( $K = 0$ ) is located at 68.264 MHz for  $H = 6.10$  T. The green inverse triangles represent the electric quadrupole splitting. (b) Temperature  $T$  dependence of integrated spin-echo intensity  $I$  multiplied by  $T$ , where  $I$  is extrapolated to  $\tau = 0$  by measuring the spin-echo decay rate  $T_2^{-1}$  using the pulse sequence of  $(\pi/2)-\tau-(\pi/2)-\tau$ , and (c) nuclear spin-lattice relaxation rate  $T_1^{-1}$  divided by  $T$  for  $x = 0$  and  $x = 0.1$ .

in symmetry. An additional line at a higher frequency side [a red inverse triangle in Fig. 5(a)] possibly originates from some of the V3 sites, which become nonmagnetic through the formation of a strong trimer or tetramer. Below  $T_{\text{tr}}$ , the quadrupole splitting is enhanced and partly resolved with a splitting frequency of 0.1 MHz, which suggests  $d$  orbital ordering.

Unlike in the case of bulk susceptibility, a weak temperature variation is observed in the Knight shift for the main peak. Therefore, the observed V sites (V2) have vanishing spin susceptibility, and the other V sites (V1 and V3) dominate the bulk susceptibility. The integrated spectral intensity  $I$  multiplied by temperature  $T$  abruptly increases below

$T_{\text{tr}}$  [Fig. 5(b)]. This means that the number of nonmagnetic V sites increases below  $T_{\text{tr}}$ , consistent with the suppression of bulk susceptibility. We observed a similar behavior for  $x = 0.1$ .

The nuclear spin-lattice relaxation rate divided by temperature,  $(T_1T)^{-1}$ , is a measure of the density of states,  $N$ , in the Korringa's law for itinerant systems,  $(T_1T)^{-1} \propto N^2$ . As shown in Fig. 5(c), we observed a constant behavior of  $(T_1T)^{-1}$  for each phase and a stepwise decrease in  $(T_1T)^{-1}$  across the phase transitions. In the LT phase,  $(T_1T)^{-1}$  is suppressed to  $\sim 10\%$  of the HT phase value, corresponding to the residual density of states of  $\sim 30\%$ . This result supports the reduction in carrier (electron) density through valence bond formations of all V sites and orbital ordering at  $T_{\text{tr}}$ , as exemplified in the  $T$  dependence of the Hall coefficient (Fig. 4).

## V. OPTICAL MEASUREMENT

Figures 6 (a) and (b) show the optical conductivity spectra along the  $ab$  plane [ $\sigma_a(\omega)$ ] and  $c$ -axis [ $\sigma_c(\omega)$ ] for  $\text{Ba}_{0.9}\text{Sr}_{0.1}\text{V}_{13}\text{O}_{18}$  (exhibiting the HT, IT, and LT phases) and  $\text{SrV}_{13}\text{O}_{18}$  (exhibiting the HT and LT phases) at 300 K up to 5 eV, respectively. There are three structures in all the spectra. The peak below 1 eV can be assigned to the excitation of the  $d$  electrons between the V ions with different valences [mainly from  $\text{V}^{2+} (3d^3)$  to  $\text{V}^{3+} (3d^2)$ ], which is called in-gap excitation. The broad peak centered at 2 eV can be assigned to the Mott-gap excitation, which is the excitation of the  $d$  electrons between the V ions with the same valence [mainly from  $\text{V}^{3+} (3d^2)$  to  $\text{V}^{3+} (3d^2)$ ]. The structures above 3.5 eV can be attributed to the charge-transfer excitation, which is the excitation from the oxygen  $2p$  state to the V  $d$  state. This is similar to the spectrum for  $\text{BaV}_{13}\text{O}_{18}$  (exhibiting only the HT and IT phases) previously reported.<sup>12</sup>

Figures 7 (a) and (b) show the  $\sigma_a(\omega)$  and  $\sigma_c(\omega)$  spectra of  $\text{Ba}_{0.9}\text{Sr}_{0.1}\text{V}_{13}\text{O}_{18}$  below 1 eV at various temperatures. With decreasing  $T$ , the peak at  $\sim 0.1$  eV in both  $\sigma_a(\omega)$  and  $\sigma_c(\omega)$  shifts to a higher frequency across  $T_{\text{co}}$  (from the HT phase to the IT phase). This spectral change is similar to that of  $\text{BaV}_{13}\text{O}_{18}$  exhibiting only the HT and IT phases previously reported.<sup>12</sup> With further decrease in  $T$ , the peak in  $\sigma_a(\omega)$  (0.3 eV at 90 K) decreases and broadens below  $T_{\text{tr}} = 80$  K (from the IT phase to the LT phase). With this peak broadening,  $\sigma_a(\omega)$  below 0.1 eV increases below  $T_{\text{tr}}$ . This is consistent with the decrease in  $\rho_a(T)$  (increase

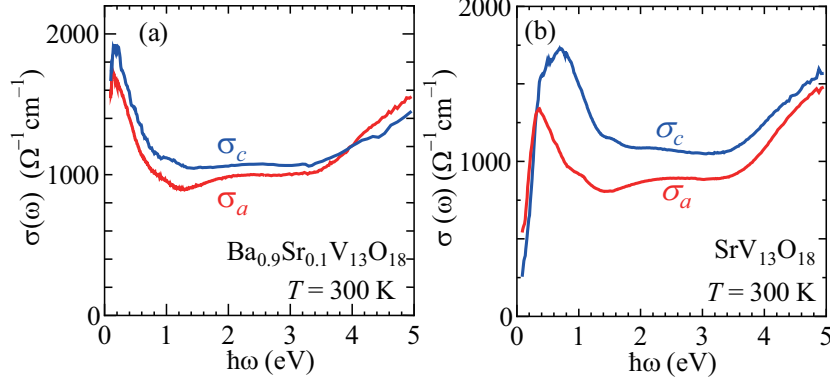


FIG. 6: (Color online) (a) Optical conductivity spectra along  $ab$  plane [ $\sigma_a(\omega)$ ] and  $c$ -axis [ $\sigma_c(\omega)$ ] at 300 K for (a)  $\text{Ba}_{0.9}\text{Sr}_{0.1}\text{V}_{13}\text{O}_{18}$  and (b)  $\text{SrV}_{13}\text{O}_{18}$ .

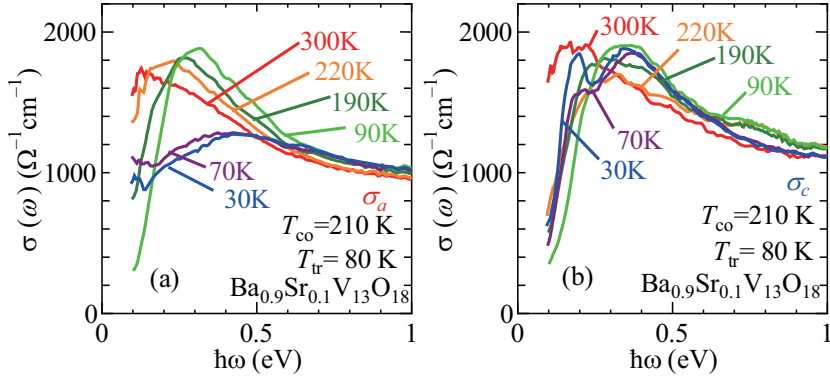


FIG. 7: (Color online) Optical conductivity spectra along (a)  $ab$  plane [ $\sigma_a(\omega)$ ] and (b)  $c$ -axis [ $\sigma_c(\omega)$ ] for  $\text{Ba}_{0.9}\text{Sr}_{0.1}\text{V}_{13}\text{O}_{18}$  at various temperatures.

in dc conductivity) below  $T_{\text{tr}}$  [Fig. 3(b)]. On the other hand, the peak in  $\sigma_c(\omega)$  ( $\sim 0.4$  eV at 90 K) splits into two peaks at 0.2 and 0.4 eV, but the suppression of the spectral weight at low frequencies survives even below  $T_{\text{tr}}$ , consistent with the increase in  $\rho_c(T)$  below  $T_{\text{tr}}$  [Fig. 3(b)].

To see the change in electronic structure more clearly, the spectral weights for  $\text{Ba}_{0.9}\text{Sr}_{0.1}\text{V}_{13}\text{O}_{18}$  were obtained by integrating  $\sigma_a(\omega)$  and  $\sigma_c(\omega)$  between 0.1 and 0.2 eV, and between 0.1 and 0.5 eV, and are plotted as a function of  $T$  in Figs. 8 (a) and (b). The spectral weight for  $\sigma_a(\omega)$  up to 0.2 eV begins to decrease below  $T_{\text{co}}$  [Fig. 8(a)], whereas that for both  $\sigma_a(\omega)$  and  $\sigma_c(\omega)$  up to 0.5 eV barely changes at  $T_{\text{co}}$  [Fig. 8(b)]. With further decrease in  $T$ , the spectral weight for  $\sigma_a(\omega)$  up to 0.5 eV decreases at  $T_{\text{tr}}$  [Fig. 8(b)]. These

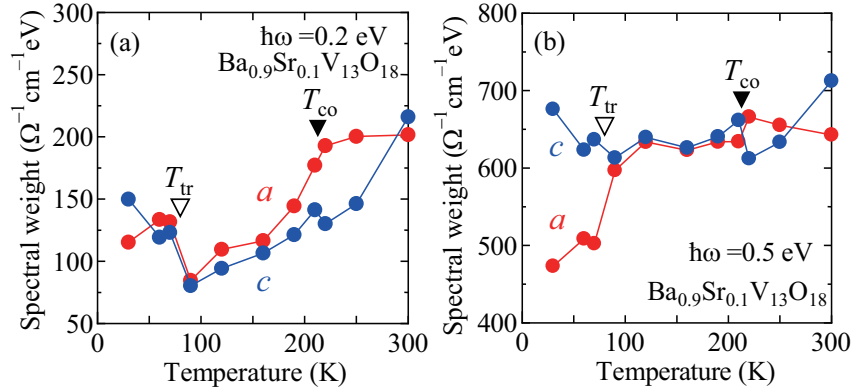


FIG. 8: (Color online) Temperature dependence of spectral weight (a) between 0.1 and 0.2 eV, and (b) between 0.1 and 0.5 eV.

results indicate that the spectral weight transfer associated with the transition from the HT phase to the IT phase occurs only below 0.5 eV, whereas that with the transition from the IT phase to the LT phase extends over the energy scale higher than 0.5 eV. Note that a similar change in the optical conductivity spectrum over the energy scale much higher than 0.5 eV is observed in  $\text{BaV}_{10}\text{O}_{15}$ ,<sup>6</sup> which exhibits a phase transition with the V trimerization caused by the orbital ordering of V  $t_{2g}$  states, similarly to the LT phase in the present compound.

To see the anisotropy of optical conductivity, the  $\sigma_a(\omega)$  and  $\sigma_c(\omega)$  spectra at the same temperature (300, 160, or 30 K) for  $\text{Ba}_{0.9}\text{Sr}_{0.1}\text{V}_{13}\text{O}_{18}$  are compared in the same panel in Fig. 9. As can be seen,  $\sigma_a(\omega)$  and  $\sigma_c(\omega)$  are similar at 300 K (in the HT phase) and 160 K (in the IT phase), but the peak in  $\sigma_c(\omega)$  below 1 eV is discernibly higher than that in  $\sigma_c(\omega)$  at 30 K (in the LT phase). As discussed above, the optical conductivity spectra below 1 eV should be attributed to the in-gap excitation between the V ions with different valences. Such an excitation is possible within the V tetramer consisting of  $\text{V}^{2+}$  and  $\text{V}^{3+}$  [Fig. 2(b)], but not within the V trimer consisting of only  $\text{V}^{3+}$  ions [Fig. 2(a)]. In the LT phase, the three V trimers do not contribute to the in-gap excitation and only the V tetramer does. Since the normal axis of the tetramer is away from the *c*-axis by  $\sim 70^\circ$  [Fig. 2(c)], the spectral weight for the in-gap excitation is expected to be larger for  $\sigma_c(\omega)$ . This can explain the peak in  $\sigma_c(\omega)$  being larger than that in  $\sigma_a(\omega)$  below 1 eV. On the other hand, the nearly isotropic spectra in the IT and HT phases indicate that, although the charge and orbital ordering occurs also in the V tetramer in the IT and HT phases, the charge and orbital modulations are not as large as those in the LT phase for  $\text{Ba}_{0.9}\text{Sr}_{0.1}\text{V}_{13}\text{O}_{18}$ . The appearance of the anisotropy in

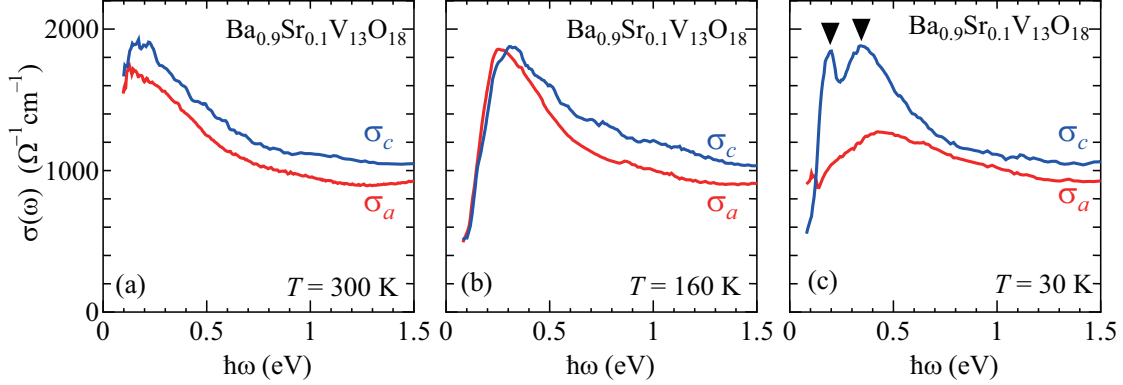


FIG. 9: (Color online) (a)(b)(c)  $\sigma_a(\omega)$  and  $\sigma_c(\omega)$  spectra at (a) 300 K (HT phase), (b) 160 K (IT phase), and (c) 30 K (LT phase).

the optical spectra associated with the charge/orbital ordering has been observed in various compounds, for example, Ru oxides<sup>23,24</sup>, V oxides<sup>25–27</sup>, and Mn oxides<sup>28–31</sup>.

Note that the anisotropy of the peak in the conductivity spectrum below 1 eV in the LT phase shown in Fig. 9 (c) ( $\sigma_c > \sigma_a$ ) is opposite to that in the dc resistivity ( $\rho_c > \rho_a$ ) shown in Fig. 3(b). The latter is consistent with the  $\sigma_c(\omega)$  and  $\sigma_a(\omega)$  spectra that cross at  $\sim 0.1$  eV and the relation  $\sigma_a(\omega) > \sigma_c(\omega)$  below 0.1 eV. This indicates that the itinerant carriers that contribute to the dc conduction and the in-gap excitation between  $V^{2+}$  and  $V^{3+}$  in the V trimer and V tetramer and the one-dimensional band along the  $ab$  plane composed of the  $d$  states in the V ions that do not contribute to the bond formation can coexist in the LT phase of this series of compounds. Such a one-dimensional band can explain the lower dc resistivity along the  $ab$  plane experimentally observed.

Figures 10 (a) and (b) show the optical conductivity spectra of  $SrV_{13}O_{18}$ , which exhibit the transition from the HT phase to the LT phase at  $T_{tr} = 270$  K (without the IT phase), at various temperatures. With decreasing  $T$ , the peak at  $\sim 0.3$  eV in  $\sigma_a(\omega)$  gradually decreases, but  $\sigma_a(\omega)$  below 0.15 eV remains as it is or rather increases. On the other hand, in  $\sigma_c(\omega)$ , the peaks at  $\sim 0.3$  and  $\sim 0.7$  eV gradually decrease with decreasing  $T$  and the spectral weight below  $\sim 0.2$  eV is suppressed at 50 K. This result is consistent with the resistivity behavior;  $\rho_c$  continuously increases below  $T_{tr}$ , whereas  $\rho_a$  is almost  $T$ -independent.

The spectral weight for  $SrV_{13}O_{18}$  between 0.1 and 1 eV is plotted as a function of  $T$  in Fig. 11. At  $T_{tr}$ , the spectral weight for  $\sigma_c(\omega)$  starts to decrease, whereas that for  $\sigma_a(\omega)$  is almost

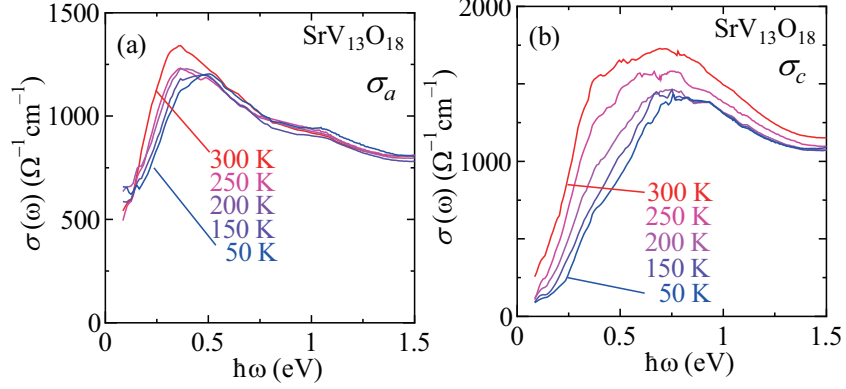


FIG. 10: (Color online) (a)  $\sigma_a(\omega)$  and (b)  $\sigma_c(\omega)$  spectra for  $\text{SrV}_{13}\text{O}_{18}$  at various temperatures.

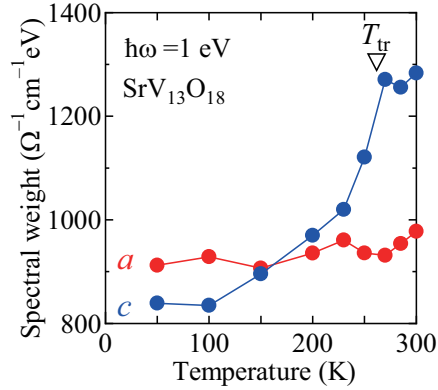


FIG. 11: (Color online) Temperature dependence of spectral weight for  $\sigma_a(\omega)$  (red circles) and  $\sigma_c(\omega)$  (blue circles) between 0.1 and 1 eV .

$T$ -independent. This result indicates that the reconstruction of the electronic structure with the V trimerization occurs over 1 eV in  $\text{SrV}_{13}\text{O}_{18}$ , whose energy scale is higher than that in  $\text{Ba}_{0.9}\text{Sr}_{0.1}\text{V}_{13}\text{O}_{18}$ .

The  $\sigma_a(\omega)$  and  $\sigma_c(\omega)$  spectra at the same  $T$  [300K (HT phase) and 50 K (LT phase)] for  $\text{SrV}_{13}\text{O}_{18}$  are compared in Fig. 12. At 50 K (in the LT phase), the peak in  $\sigma_c$  is larger than that in  $\sigma_a$ , similarly to that observed in  $\text{Ba}_{0.9}\text{Sr}_{0.1}\text{V}_{13}\text{O}_{18}$ . However,  $\sigma_c(\omega)$  is larger than  $\sigma_a(\omega)$  above 0.2 eV even in the HT phase for  $\text{SrV}_{13}\text{O}_{18}$ , and this is in contrast to the nearly isotropic spectra in the HT and IT phases for  $\text{Ba}_{0.9}\text{Sr}_{0.1}\text{V}_{13}\text{O}_{18}$ . This is possibly explained by the fact that the V–V bonds in the V tetramer of  $\text{SrV}_{13}\text{O}_{18}$  are shorter than those of  $\text{Ba}_{0.9}\text{Sr}_{0.1}\text{V}_{13}\text{O}_{18}$  because of the smaller lattice constants (caused by the smaller ionic radius of Sr), giving rise to the larger charge and orbital modulations in the V tetramer and the

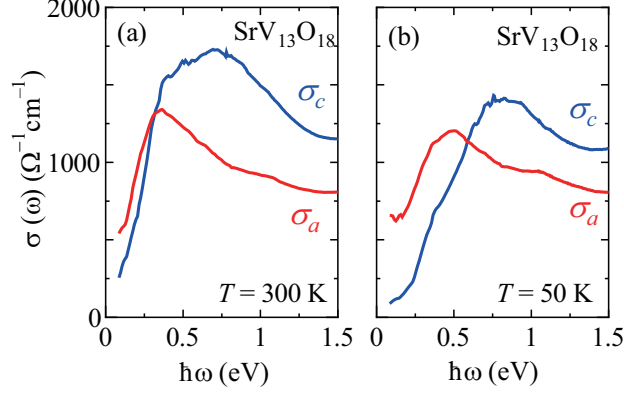


FIG. 12: (Color online) (a)(b)  $\sigma_a(\omega)$  and  $\sigma_c(\omega)$  spectra at (a) 300 K (HT phase) and (c) 50 K (LT phase) for  $\text{SrV}_{13}\text{O}_{18}$ .

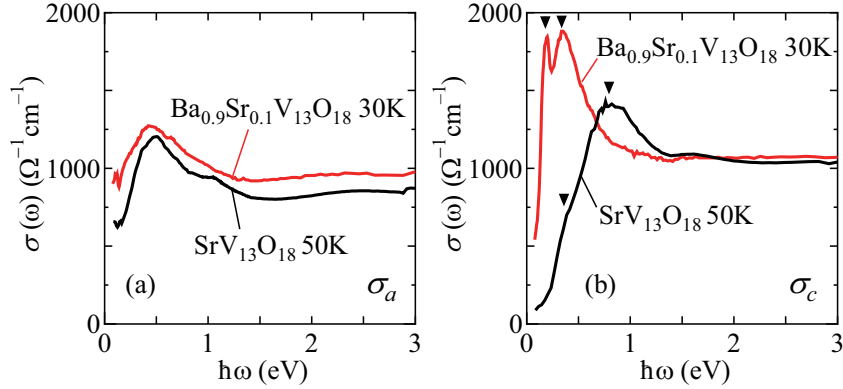


FIG. 13: (Color online) The comparison of (a)  $\sigma_a(\omega)$  and (c)  $\sigma_c(\omega)$  at the lowest temperature between  $\text{Ba}_{0.9}\text{Sr}_{0.1}\text{V}_{13}\text{O}_{18}$  and  $\text{SrV}_{13}\text{O}_{18}$ .

anisotropy of the electronic structure of  $\text{SrV}_{13}\text{O}_{18}$ .

Finally, let us compare the optical conductivity spectra of  $\text{Ba}_{0.9}\text{Sr}_{0.1}\text{V}_{13}\text{O}_{18}$  and  $\text{SrV}_{13}\text{O}_{18}$  at the lowest  $T$  (Fig. 13). The  $\sigma_c(\omega)$  spectra of both  $\text{Ba}_{0.9}\text{Sr}_{0.1}\text{V}_{13}\text{O}_{18}$  and  $\text{SrV}_{13}\text{O}_{18}$  exhibit similar suppression of the spectral weight at low frequencies, but the energy scale in the suppression of  $\sigma_c(\omega)$  is discernibly larger for  $\text{SrV}_{13}\text{O}_{18}$ . Furthermore, the two peaks at 0.2 and 0.4 eV in the  $\sigma_c(\omega)$  spectrum for  $\text{Ba}_{0.9}\text{Sr}_{0.1}\text{V}_{13}\text{O}_{18}$  shift to higher frequencies at 0.4 and 0.8 eV for  $\text{SrV}_{13}\text{O}_{18}$ . As discussed above, the conductivity spectrum in this frequency range is dominated by the in-gap excitation between  $\text{V}^{2+}$  and  $\text{V}^{3+}$  existing in the V tetramer. We speculate that the shorter V–V bonds in the V tetramer in  $\text{SrV}_{13}\text{O}_{18}$  than in  $\text{Ba}_{0.9}\text{Sr}_{0.1}\text{V}_{13}\text{O}_{18}$  cause the larger charge and orbital modulations, resulting in a larger charge gap. On the

other hand, the  $\sigma_a(\omega)$  spectra of  $\text{Ba}_{0.9}\text{Sr}_{0.1}\text{V}_{13}\text{O}_{18}$  and  $\text{SrV}_{13}\text{O}_{18}$  are similar up to 3 eV. These behaviors are consistent with those of  $\rho_a(T)$  and  $\rho_c(T)$  shown in Fig. 3;  $\rho_c$  at the lowest  $T$  varies from  $3 \times 10^{-3} \Omega\text{cm}$  to  $20 \times 10^{-3} \Omega\text{cm}$  with  $x$  whereas  $\rho_a$  is within  $2 \sim 4 \times 10^{-3} \Omega\text{cm}$  irrespective of  $x$ .

## VI. SUMMARY

We measured the electrical resistivity, Hall coefficient, magnetic susceptibility, NMR, and optical reflectivity of  $\text{Ba}_{1-x}\text{Sr}_x\text{V}_{13}\text{O}_{18}$  single crystals, which have orbital and charge degrees of freedom, and exhibit three phases (HT, IT, and LT phases) for  $x \leq 0.3$  and two phases (HT and LT phases) for  $x > 0.3$ . We found large changes in various quantities with a phase transition into the LT phase. We also found that anisotropy in the electronic structure is enhanced in the LT phase. These results can be attributed to the orbital ordering of the V  $t_{2g}$  states associated with the formation of the V tetramers and trimers in the LT phase of this series of compounds.

## VII. ACKNOWLEDGMENT

This work was supported by JSPS KAKENHI Grant No. 16H04020, JP16H04012, and by JST CREST Grant No. JPMJCR15Q2.

- 
- <sup>1</sup> P. F. Bongers, Ph. D. Thesis, University of Leiden (1957).
  - <sup>2</sup> K. Kobayashi, K. Kosuge, and S. Kachi, Mater. Res. Bull. **4**, 95 (1969).
  - <sup>3</sup> W. Tian, M. Chisholm, P. Khalifah, R. Jin, B. Sales, S. Nagler, and D. Mandrus, Mater. Res. Bull. **39**, 1319 (2004).
  - <sup>4</sup> H. F. Pen, J. van den Brink, D. I. Khomskii, and G. A. Sawatzky, Phys. Rev. Lett. **78**, 1323 (1997).
  - <sup>5</sup> C. Bridges and J. Greedan, J. Solid State Chem. **177**, 1098 (2004).
  - <sup>6</sup> T. Kajita, T. Kanzaki, T. Suzuki, J. E. Kim, K. Kato, M. Takata, and T. Katsufuji, Phys. Rev. B **81**, 060405(R) (2010).

- <sup>7</sup> Y. Shimizu, K. Matsudaira, M. Itoh, T. Kajita, and T. Katsufuji, *Phys. Rev. B* **84**, 064421 (2011).
- <sup>8</sup> K. Takubo, T. Kanzaki, Y. Yamasaki, H. Nakao, Y. Murakami, T. Oguchi, and T. Katsufuji, *Phys. Rev. B* **86**, 085141 (2012).
- <sup>9</sup> J. Miyazaki, K. Matsudaira, Y. Shimizu, M. Itoh, Y. Nagamine, S. Mori, J. E. Kim, K. Kato, M. Takata, and T. Katsufuji, *Phys. Rev. Lett.* **104**, 207201 (2010).
- <sup>10</sup> M. Ikeda, Y. Nagamine, S. Mori, J. E. Kim, K. Kato, M. Takata, and T. Katsufuji, *Phys. Rev. B* **82**, 104415 (2010).
- <sup>11</sup> M. Ikeda, T. Okuda, K. Kato, M. Takata, and T. Katsufuji, *Phys. Rev. B* **83**, 134417 (2011).
- <sup>12</sup> T. Kanzaki, J. Fujioka, Y. Tokura, H. Kuwahara, and T. Katsufuji, *Phys. Rev. B* **89**, 140401 (2014).
- <sup>13</sup> K. Momma and F. Izumi, *J. Appl. Cryst.* **44**, 1272 (2011).
- <sup>14</sup> T. Jin-no, Y. Shimizu, M. Itoh, S. Niitaka, and H. Takagi, *Phys. Rev. B* **87**, 075135 (2013).
- <sup>15</sup> E. D. Jones, *Phys. Rev.* **137**, A978 (1965).
- <sup>16</sup> H. N. S. Lee, H. McKinzie, D. S. Tannhauser, and A. Wold, *J. Appl. Phys.* **40**, 602 (1969).
- <sup>17</sup> M. Naito and S. Tanaka, *J. Phys. Soc. Jpn.* **51**, 219 (1982).
- <sup>18</sup> N. Shirakawa, K. Murata, Y. Nishihara, S. Nishizaki, Y. Maeno, T. Fujita, J. G. Bednorz, F. Lichtenberg, and N. Hamada, *J. Phys. Soc. Jpn.* **64**, 1072 (1995).
- <sup>19</sup> A. P. Mackenzie, N. E. Hussey, A. J. Diver, S. R. Julian, Y. Maeno, S. Nishizaki, and T. Fujita, *Phys. Rev. B* **54**, 7425 (1996).
- <sup>20</sup> L. M. Galvin, R. S. Perry, A. W. Tyler, A. P. Mackenzie, S. Nakatsuji, and Y. Maeno, *Phys. Rev. B* **63**, 161102 (2001).
- <sup>21</sup> G. Cao, S. McCall, M. Shepard, J. E. Crow, and R. P. Guertin, *Phys. Rev. B* **56**, 321 (1997).
- <sup>22</sup> Y. Klein, G. Rousse, F. Damay, F. Porcher, G. André, and I. Terasaki, *Phys. Rev. B* **84**, 054439 (2011).
- <sup>23</sup> S. J. Moon, W. S. Choi, S. J. Kim, Y. S. Lee, P. G. Khalifah, D. Mandrus, and T. W. Noh, *Phys. Rev. Lett.* **100**, 116404 (2008).
- <sup>24</sup> C. Mirri, L. Baldassarre, S. Lupi, M. Ortolani, R. Fittipaldi, A. Vecchione, and P. Calvani, *Phys. Rev. B* **78**, 155132 (2008).
- <sup>25</sup> S. Miyasaka, Y. Okimoto, and Y. Tokura, *J. Phys. Soc. Jpn.* **71**, 2086 (2002).
- <sup>26</sup> J. Fujioka, S. Miyasaka, and Y. Tokura, *Phys. Rev. Lett.* **97**, 196401 (2006).

- <sup>27</sup> J. Fujioka, S. Miyasaka, and Y. Tokura, Phys. Rev. B **77**, 144402 (2008).
- <sup>28</sup> T. Ishikawa, T. Kimura, T. Katsufuji, and Y. Tokura, Phys. Rev. B **57**, R8079 (1998).
- <sup>29</sup> T. Ishikawa, K. Tobe, T. Kimura, T. Katsufuji, and Y. Tokura, Phys. Rev. B **62**, 12354 (2000).
- <sup>30</sup> J. H. Jung, D.-W. Kim, T. W. Noh, H. C. Kim, H.-C. Ri, S. J. Levett, M. R. Lees, D. M. Paul, and G. Balakrishnan, Phys. Rev. B **64**, 165106 (2001).
- <sup>31</sup> K. Tobe, T. Kimura, and Y. Tokura, Phys. Rev. B **69**, 014407 (2004).